MUSCULOSKELETAL

Peripheral nerve sheath tumor: differentiation of malignant from benign tumors with conventional and diffusion-weighted MRI

Jae Sung Yun[1,2] · Min Hee Lee[1] · Seung Min Lee[1,3] · Jong Seok Lee[4] · Hwa Jung Kim[5,6] · Sun Joo Lee[7] ·
Hye Won Chung[1] · Sang Hoon Lee[1] · Myung Jin Shin[1]

Abstract

Objectives To evaluate potential of conventional MRI and diffusion-weighted imaging (DWI) for differentiating malignant from benign peripheral nerve sheath tumors (PNSTs).

Methods Eighty-seven cases of malignant or benign PNSTs in the trunk or extremities that underwent conventional MRI with contrast enhancement, DWI, and pathologic confirmation between Sep. 2014 and Dec. 2017 were identified. Of these, 55 tumors of uncertain nature on MRI were included. Tumor size, signal, and morphology were reviewed on conventional MRI, and apparent diffusion coefficient (ADC) values of solid enhancing portions were measured from DWI. Patient demographics, MRI features, and ADC values were compared between benign and malignant tumors, and robust imaging findings for malignant peripheral nerve sheath tumors (MPNSTs) were identified using multivariable models.

Results A total of 55 uncertain tumors consisted of 18 malignant and 37 benign PNSTs. On MRI, tumor size, margin, perilesional edema, and presence of split fat, fascicular, and target signs were significantly different between groups ($p < 0.05$), as were mean and minimum ADC values ($p = 0.002$, $p < 0.0001$). Most inter-reader agreement was moderate to excellent (κ value, 0.45–1.0). The mean ADC value and absence of a split fat sign were identified as being associated with MPNSTs (odds ratios = 13.19 and 25.67 for reader 1; 49.05 and 117.91 for reader 2, respectively). The C-indices obtained by combining these two findings were 0.90 and 0.95, respectively.

Conclusions Benign and malignant PNSTs showed different features on MRI and DWI. A combination of mean ADC value and absence of split fat was excellent for discriminating malignant from benign PNSTs.

Key Points
• *It is important to distinguish between malignant peripheral nerve sheath tumors (MPNSTs) and benign peripheral nerve sheath tumors (BPNSTs) to ensure an appropriate treatment plan.*
• *On conventional MRI and diffusion-weighted imaging (DWI), MPNSTs and BPNSTs showed significant differences in tumor size, margin, presence of perilesional edema, and absence of split fat, fascicular, and target signs.*
• *Absence of a split fat sign and mean apparent diffusion coefficient (ADC) values were robust imaging findings distinguishing MPNSTs from BPNSTs, with a C-index of > 0.9.*

Keywords Malignant peripheral nerve sheath tumor · Diffusion magnetic resonance imaging · Magnetic resonance imaging

✉ Min Hee Lee
mhlee625@gmail.com

1 Department of Radiology and Research Institute of Radiology, University of Ulsan College of Medicine, Asan Medical Center, 88 Olympic-ro, 43-gil, Songpa-gu, Seoul 05505, South Korea

2 Department of Radiology, Ajou University School of Medicine, Suwon, South Korea

3 Department of Radiology, Leaders Hospital, Seoul, South Korea

4 Department of Orthopedic Surgery, University of Ulsan College of Medicine, Asan Medical Center, Seoul, South Korea

5 Department of Preventive Medicine, University of Ulsan College of Medicine, Seoul, South Korea

6 Department of Clinical Epidemiology and Biostatics, Asan Medical Center, Seoul, South Korea

7 Department of Radiology, Busan Paik Hospital, Inje University College of Medicine, Busan, South Korea

Abbreviations

ADC	Apparent diffusion coefficient
AUC	Area under the curve
BPNSTs	Benign peripheral nerve sheath tumors
CEFST1WI	Contrast-enhanced fat-suppressed T1-weighted imaging
DWI	Diffusion-weighted imaging
MPNSTs	Malignant peripheral nerve sheath tumors
MRI	Magnetic resonance imaging
NF-1	Neurofibromatosis type 1
OR	Odds ratio
ROC	Receiver operating characteristic
ROIs	Regions of interest

Introduction

Neurogenic neoplasms including traumatic neuroma, Morton's neuroma, neural fibrolipoma, nerve sheath ganglion, and peripheral nerve sheath tumors are commonly encountered in daily practice [1]. Among them, benign peripheral nerve sheath tumors (BPNSTs), which can be divided into schwannoma and neurofibroma, account for 10–12% of the benign soft tissue tumors occurring in the general population. However, malignant peripheral nerve sheath tumors (MPNSTs) are relatively rare, with an incidence ranging from 3 to 10% of soft tissue sarcomas, giving consideration to their higher prevalence in patients with neurofibromatosis type 1 (NF-1) [2, 3]. The differentiation of benign from malignant PNSTs is important for appropriate management plans, and as MPNST is highly malignant with a tendency for recurrence and metastasis, its early diagnosis is necessary. When it is certain that a mass is benign, which is the case for most sporadic neurogenic tumors, follow-up and monitoring are reasonable management options. Otherwise, indeterminate lesions, for which there is uncertainty as to whether they are benign or malignant, require subsequent biopsy or surgical removal for accurate histological diagnosis [4]. Unfortunately, biopsy of these tumors may cause severe pain, nerve palsy, or even seeding of malignant tumor cells into visceral organs [5].

Magnetic resonance imaging (MRI) plays a central role in the evaluation and monitoring of soft tissue tumors, and also in biopsy planning. There have been previous studies investigating the use of imaging morphology for the differentiation of benign from malignant PNSTs [6–9], and these have mostly suggested that some imaging features are helpful for distinguishing the tumor types, but they have not stated a single or combination of findings that can provide a more definite determination. Over the last decade, diffusion-weighted imaging (DWI) has been reported as a useful supplemental technique to conventional MRI for the differentiation of benign from malignant soft tissue tumors, as it provides additional information reflecting the cellularity of tumors, which is represented by water diffusivity in the tissue. A recent study by Demehri et al suggested that minimum apparent diffusion coefficient (ADC) values on DWI along with average tumor diameter could be useful for differentiating BPNSTs from MPNSTs [10].

In this study, we evaluated conventional MRI and DWI of malignant and benign PNSTs of an uncertain nature, and assessed the independent imaging findings on MRI and DWI that were associated with MPNSTs. If possible, accurate characterization of PNSTs by a noninvasive imaging technique could avoid unnecessary biopsies of benign tumors.

Materials and methods

Study population

This retrospective study was approved by our institutional review board, and the requirement for informed consent was waived. Eighty-seven cases of malignant or benign PNSTs located in the trunk and extremities of 83 patients between Sep. 2014 and Dec. 2017 were enrolled in this study. These PNSTs were confirmed histologically by either surgical excision or ultrasound-guided core needle biopsy at one of two different tertiary institutions. The patients underwent preoperative conventional MRI examinations with intravenous contrast enhancement and DWI. Of the total 87 cases, 32 cases of tumors presumed to be definitely benign (maximum size < 3 cm, well-defined margin, a target sign, homogeneous signal intensity, and the absence of necrosis in NF-1) based on findings of previous reports [5, 10]; recurrent tumors after surgical removal; and infiltrative subcutaneous lesions indicating neurofibroma were excluded from further analysis. Finally, the remaining 55 cases in 51 patients, which included 24 men (mean age, 42.6 years; range, 16–72 years) and 27 women (mean age, 54.7 years; range, 16–85 years), were included in this study. Sixteen masses were located in an upper extremity, 23 in a lower extremity, and 16 in the trunk. Of the 55 cases, 18 were malignant and 37 were benign. Table 1 summarizes the demographic characteristics of the patients.

MRI examination

All patients underwent MRI examinations on a 1.5-T (Achieva, Philips Healthcare [$n = 1$]; or Magnetom Avanto, Siemens Healthineers [$n = 1$]) or 3-T (Ingenia or Achieva, Philips Healthcare [$n = 18$ and 19, respectively]; or Magnetom Skyra, Siemens Healthineers [$n = 16$]) scanner, with adjustments to the coils, field of view, and matrix depending on the tumor location. The acquisition parameters varied depending on the anatomical region and the referral base of each institution; however, all patients in this study

Table 1 Demographic characteristics of the patients with benign and malignant peripheral nerve sheath tumors

Clinical data	MPNST ($n = 18$)	BPNST ($n = 37$)
No. of patients	17	34*
Median age (years), (range)	51.1 (16–85)	48.3 (16–71)
Sex		
Men	8	18
Women	10	19
Underlying NF-1	6	9
Benign pathologies		Schwannoma ($n = 30$) Neurofibroma ($n = 7$)

MPNST, malignant peripheral nerve sheath tumor; *BPNST*, benign peripheral nerve sheath tumor; *NF-1*, neurofibromatosis type 1

*One patient had three benign neurogenic tumors and one patient had two benign neurogenic tumors

underwent axial and either coronal or sagittal T1-weighted imaging prior to injection of intravenous contrast material, axial and either coronal or sagittal T2-weighted imaging with or without fat saturation, and contrast-enhanced fat-suppressed T1-weighted imaging (CEFST1WI) in all three planes (Gadovist, Bayer; or Dotarem, Guerbet). Before contrast enhancement, DWI was performed in the axial plane using a spin-echo single-shot echo-planar imaging sequence with *b*-values of 0, 400, and 800 s/mm^2. ADC maps were automatically constructed using a mono-exponential calculation from

the DWI. Table 2 summarizes the detailed parameters for each MRI sequence.

MRI analysis

Two musculoskeletal radiologists (reader 1 with 20 years and reader 2 with 2 years of experience in musculoskeletal radiology), who were blinded to the clinical information and histologic findings, interpreted the MRI features independently, assessing signal heterogeneity (homogeneous or heterogeneous) on T1- and T2-weighted images, shape (round/ovoid, irregular), and margin (well-defined; partly well-defined, > 70% of margin well-defined; ill-defined, < 70% of margin well-defined). The presence or absence of the split fat sign, fascicular sign, target sign, peritumoral edema, eccentricity to the nerve, and intratumoral hemorrhage/cystic change were recorded. The effects on the adjacent bone (no effect, remodeling, destruction) were also evaluated. The presence or absence of tumor enhancement on CEFST1WI was evaluated, and if present, the percentage of tumor enhancement (< 10%, 11–50%, and > 50%) was recorded.

A third independent radiologist (with 2 years of experience in musculoskeletal radiology) evaluated ADC values and tumor size on MRI. The tumor maximum diameter was measured in three planes (craniocaudal, anteroposterior, and transverse), and the average diameter of each tumor was calculated. ADC values were obtained from one representative axial

Table 2 MR imaging sequence parameters

Parameters	3-T MRI		1.5-T MRI	
	Conventional MRI	DWI	Conventional MRI	DWI
Repetition time (ms)/echo time (ms)	T1-weighted coronal or sagittal imaging: 450–641/12–22 T2-weighted coronal or sagittal imaging: 2044–6290/62–100 T1-weighted axial imaging: 436–648/12–21 T2-weighted axial imaging: 2090–9783/62–100	4093–8083/55–115	T1-weighted coronal or sagittal imaging: 480–580/10–20 T2-weighted coronal or sagittal imaging: 2670–6000/50–120 T1-weighted axial imaging: 507–536/10–20 T2-weighted axial imaging: 2670–6000/50–120	2612–4000/66–69
Fat suppression	SPAIR	SPAIR	SPAIR	SPAIR
Echo-planar imaging factor	NA	67	NA	150
Field of view (mm)	Sagittal imaging: 180–635 Axial imaging: 150–250 Coronal imaging: 150–635	150–250	Sagittal imaging: 270–300 Axial imaging: 170–280 Coronal imaging: 208–360	300–340
Section thickness (mm)	2.5–4	3–5	3	3
Intersection gap (mm)	0–4	0–4	0–1	0
Matrix size	208 × 208–516 × 516	80 × 80–160 × 160	384 × 381–512 × 512	256 × 256
Turbo factor	T1-weighted imaging: 3–5 T2-weighted imaging: 8–17	NA	T1-weighted imaging: 4 T2-weighted imaging: 8–15	NA
Number of signals acquired	1–3	1–2	1–2	4–6

SPAIR, spectral attenuated inversion recovery; *NA*, not applicable

plane. Side-by-side comparisons between conventional MR imaging and DW imaging were made when drawing the regions of interest (ROIs). ROIs were manually drawn within the solid enhancing tumor portion that also showed hyperintense signal on high b-value DWI and the most restricted area on the ADC map on visual assessment (Fig. 1) [11, 12]. The minimum and mean ADC values were recorded for each tumor using an in-house software package written as a plugin to ImageJ software (http://rsb.info.nih.gov/ij/).

Statistical analysis

Differences in the imaging characteristics between malignant and benign PNSTs were compared using Fisher's exact test for categorized variables and the Mann–Whitney U test for continuous variables. P values of < 0.05 were considered to represent significant differences. Inter-reader agreement was evaluated by kappa coefficient (κ). A κ value < 0.20 was taken to indicate poor agreement, 0.21–0.40 fair agreement, 0.41–0.60 moderate agreement, 0.61–0.80 substantial agreement, and 0.81–1.00 excellent agreement. The diagnostic performance of ADC values was assessed using receiver operating characteristic (ROC) curves, with 95% confidence intervals being used to express the statistical precision of the results. Optimal ADC threshold values were obtained using ROC curves.

Univariate and multivariable logistic regression analyses were used to identify factors independently associated with MPNSTs. To deal with rare event situations in a selected population, bootstrap methods were applied for statistical inference and confidence interval building in the regression analyses, especially the logistic regression. Variables were selected as risk factors in the logistic regression model when their relative selection frequency was more than 40% among 1000 bootstrap samples. Statistical analyses were performed with commercially available software (SPSS version 25.0, IBM Corp. and MedCalc version 18.10, MedCalc software). p values of < 0.05 were considered to represent significant differences.

Results

Table 3 summarizes the MRI features evaluated by both readers. Among the imaging features, tumor margin, perilesional edema, and the presence of a split fat sign, fascicular sign, and target sign were significantly different between MPNSTs and BPNSTs. For both readers, perilesional edema was observed in 10 MPNST cases but in none of the BPNST

Fig. 1 A 57-year-old female with a peripheral nerve sheath tumor in the right ankle. **a** Sagittal T1-weighted imaging shows a soft tissue mass encasing the tibialis anterior tendon. **b** CEFST1WI shows that the mass is mainly enhanced in the antero-medial aspect (arrows). **c** High signal intensity is visible on the medial side of the tumor on the DWI with a b-value of 800 s/mm^2 (arrows). This area is included in the solid enhancing areas on CEFST1WI. **d** Within the areas showing high signal intensity on DWI, the area that appears to be the most restricted area by visual assessment was selected as the ROI (white drawing). Areas considered as artifacts were excluded. The mean ADC value of the ROI was 0.788×10^{-3} mm^2/s. This tumor was surgically removed and pathologically confirmed as a malignant peripheral nerve sheath tumor

Table 3 Comparison of MRI features between benign and malignant peripheral nerve sheath tumors

	Reader 1			Reader 2			Kappa value
	MPNST (n = 18)	BPNST (n = 37)	p value	MPNST (n = 18)	BPNST (n = 37)	p value	
T1-weighted imaging			0.389			0.218	0.774
Homogeneous signal	10 (55.6%)	25 (67.6%)		8 (44.4%)	23 (62.3%)		
Heterogeneous signal	8 (44.4%)	12 (32.4%)		10 (55.6%)	14 (37.8%)		
T2-weighted imaging			1.000			0.485	0.000
Homogeneous signal	0 (0%)	0 (0%)		0 (0%)	1 (2.7%)		
Heterogeneous signal	18 (100%)	100% (37/37)		18 (100%)	36 (97.3%)		
Shape			0.019			0.114	0.729
Round/ovoid	12 (66.7%)	34 (91.9%)		11 (61.1%)	30 (81.1%)		
Irregular	6 (33.3%)	3 (8.1%)		7 (38.9%)	7 (18.9%)		
Margin			< 0.0001			< 0.0001	0.640
Well-defined	8 (44.4%)	37 (100%)		7 (38.9%)	94.6% (35/37)		
Partly well-defined	5 (27.8%)	0 (0%)		6 (33.3%)	5.4% (2/37)		
Ill-defined	5 (27.8%)	0 (0%)		5 (27.8%)	0% (0/37)		
Split fat sign	8 (44.4%)	35 (94.6%)	< 0.0001	5 (27.8%)	86.5% (32/37)	< 0.0001	0.639
Fascicular sign	6 (33.3%)	25 (67.6%)	0.017	5 (27.8%)	30 (81.1%)	< 0.0001	0.699
Target sign	1 (5.5%)	14 (37.8%)	0.012	2 (11.1%)	20 (54.1%)	0.003	0.640
Perilesional edema	10 (55.6%)	0 (0%)	< 0.0001	10 (55.6%)	0 (0%)	< 0.0001	1.000
Eccentric to the nerve	3 (16.7%)	20 (54.1%)	0.009	4 (22.2%)	11 (29.7%)	0.561	0.450
Enhancement			0.789			0.753	0.694
< 10	0 (0%)	0 (0%)		0 (0%)	3 (8.1%)		
11–50	6 (33.3%)	11 (29.7%)		5 (27.8%)	5 (13.5%)		
> 50	12 (66.7%)	26 (70.3%)		13 (72.2%)	29 (78.4%)		
Hemorrhage	6 (33.3%)	6 (16.2%)	0.153	5 (27.8%)	8 (27.6%)	0.617	0.845
Cystic change	9 (50%)	14 (37.8%)	0.395	5 (27.8%)	8 (27.6%)	0.617	0.522
Bone destruction			0.274			0.142	0.889
Remodeling	2 (11.1%)	4 (10.8%)		1 (5.5%)	4 (10.8%)		
Destruction	3 (16.7%)	2 (5.4%)		4 (22.2%)	1 (2.7%)		

MPNST, malignant peripheral nerve sheath tumor; BPNST, benign peripheral nerve sheath tumor

cases with a κ value of 1.0. The inter-reader agreement for MRI features was substantial to excellent, except for signal heterogeneity on T2-weighted images, eccentricity to the nerve, and intratumoral cystic change.

The maximum diameters in three planes and the average diameters were significantly larger in MPNSTs than in BPNSTs (craniocaudal, 8.6 ± 1.8 vs. 4.6 ± 2.2, $p < 0.001$; anteroposterior, 4.7 ± 3.3 vs. 3.2 ± 1.6, $p = 0.041$; transverse, 5.5 ± 0.4 vs. 3.6 ± 1.7, $p = 0.025$; average, 6.3 ± 3.4 vs. 3.8 ± 1.7, $p = 0.001$).

Both minimum and mean ADC values were significantly lower in MPNSTs than in BPNSTs (minimum ADC values, $0.73 \pm 0.47 \times 10^{-3}$ mm^2/s vs. $1.12 \pm 0.37 \times 10^{-3}$ mm^2/s, $p = 0.002$; mean ADC values, $0.94 \pm 0.37 \times 10^{-3}$ mm^2/s vs. $1.50 \pm 0.40 \times 10^{-3}$ mm^2/s, $p < 0.0001$). The AUC of the minimum ADC value was 0.759 (95% confidence interval [CI]: 0.595–0.923), while that of the mean ADC value was 0.846 (95% CI: 0.715–0.977; Fig. 2). According to the Youden index, the

minimum and mean ADC threshold values for achieving the highest diagnostic performance were 0.89×10^{-3} mm^2/s and 1.15×10^{-3} mm^2/s, respectively.

In the univariate analysis (Table 4), MPSNTs and BPNSTs showed significant differences in tumor size in the craniocaudal and transverse, and average diameters, and in the minimum and mean ADC values. For both readers, the absence of a split fat sign, fascicular sign, and target sign was significantly associated with MPNSTs. For reader 1 only, the shape and eccentricity to the nerve were significantly associated with MPNSTs, while for reader 2 only, a partly well-defined margin and bone destruction were significantly associated with MPNSTs.

The bootstrap methods identified mean ADC value and absence of a split fat sign as robust imaging findings (Table 5), and the multivariable logistic regression model was constructed using these two imaging findings (Figs. 3 and 4). The odds ratios of mean ADC values and absence of
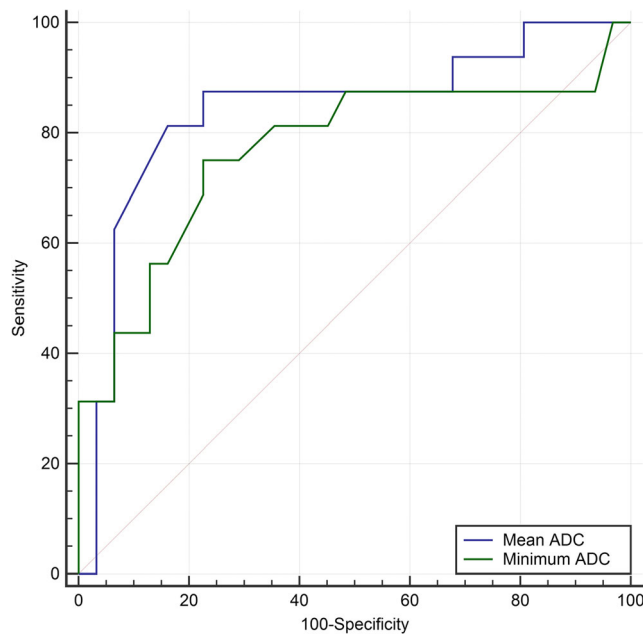
Fig. 2 Receiver operating characteristic curves comparing the diagnostic performance of the mean ADC values (area under the curve, 0.846 [95% confidence interval (CI), 0.715–0.977]) with the minimum ADC values (area under the curve, 0.759 [95% CI, 0.595–0.923]) in the assessment of MPNSTs

a split fat sign for MPNST were 25.67 (95% CI: 2.69–245.06) and 13.19 (95% CI: 1.84–94.74) for reader 1 and 117.91 (95% CI, 5.88 to > 999.99) and 49.05 (95% CI, 4.62–520.82) for reader 2. The final multivariable model demonstrated excellent discrimination ability for reader 1, reader 2, and both readers (C-index = 0.90, 0.95, and 0.92 respectively).

Discussion

In our study, tumor size, poor margin, presence of perilesional edema, absence of split fat, target, and fascicular signs, and minimum and mean ADC values were MRI and DWI features showing significant differences between benign and malignant PNSTs. These identified features are mostly consistent with previous studies [5, 7, 10, 13, 14]. We used a bootstrapping method to find imaging findings associated with MPNSTs, which identified absence of a split fat sign and mean ADC as robust imaging findings, and these were then used to construct the multivariable analysis. The combination of these two features in the multivariable models showed excellent discrimination of MPNSTs from BPNSTs, with C-indices higher than 0.9 for both readers. Bootstrapping, a resampling technique using independent sampling with replacement from existing sample data, provided a straightforward approach for calculating an approximate distribution from the empirical distribution function of the observed data [15]. We believe this method to be an appropriate metric for dealing with the imaging features of benign and malignant PNSTs, which were rare event situations in the selected population.

The split fat sign represents a rim of fat surrounding the tumor and reflects the rate at which the tumor grows. The neurovascular bundle is usually surrounded by fat in the intermuscular plane. BPNSTs arising at the neurovascular bundle maintain a rim of surrounding fat. As they slowly enlarge, the normal fat of the intermuscular space is displaced, creating a triangular fatty rind. The fatty atrophy of the surrounding muscles, caused by either a mass effect from slow growing tumors or by denervation changes, may influence the split fat sign [12]. By contrast, MPNSTs tend to be more aggressive and infiltrative in nature, resulting in the obliteration of fat at the ends of the lesion [1, 16, 17]. This suggests why the bootstrap method resulted in the absence of a split fat sign being selected as an imaging finding for MPNSTs for both readers.

Such differences in the growth patterns of BPNSTs and MPNSTs also affect the margins of the tumor and the presence of perilesional soft tissue edema [18, 19]. A previous study revealed that peritumoral infiltration of sarcomas on MRI provides information about the peripheral tumor growth, which is important for determining the prognosis and risk of metastasis [20]. In our series of 55 cases, 10 cases showing perilesional soft tissue edema were all MPNSTs, and this sign showed excellent inter-reader agreement with a κ value of 1.0 for the two readers. None of the BPNSTs showed perilesional soft tissue edema. These results are in agreement with previous studies by Wasa et al and Li et al [5, 7], who reported that lesions with perilesional edema were all MPNSTs, although perilesional edema was not seen in all MPNSTs. We assume that perilesional edema could be a useful finding for determining MPNSTs, although it could not be included in the statistical analysis because of statistical technical issues.

Histologically, neurofibromas consist of a central area of fibrocollagenous tissue and a surrounding area of myxomatous tissue. In schwannomas, more-cellular Antoni type A tissue patterns are usually distributed in the center, while less-cellular Antoni type B patterns are located in the peripheral border [16, 21]. This cellular composition in neurofibroma and schwannoma affects the MRI findings, resulting in low central and high peripheral signal intensities on T2-weighted imaging, the so-called target sign. After contrast enhancement, these tumors typically show central enhancement with peripheral hypointensity [16]. These histological characteristics also affect DWI; the peripheral area of BPNSTs, which is not well enhanced on post-contrast imaging, shows high ADC values, which likely reflect the loose acellular matrix or hypocellular Antoni B area. By contrast, the central fibrocollagenous or cellular Antoni A area may represent low ADC values. The loss of the target sign in MPNSTs may be explained by the replacement of tissue by malignant cells with increased cellularity and low diffusivity, instead of a normal cell distribution [16, 21].

Table 4 Univariate analyses for imaging findings associated with MPNSTs

Variable	Odds ratio	95% CI	C-index	Odds ratio	95% CI	C-index
Size						
Craniocaudal	1.58	1.20–2.07	0.78			
Anteroposterior	1.39	0.98–1.96	0.66			
Transverse	1.35	1.01–1.79	0.66			
Average	1.69	1.17–2.45	0.76			
Minimum ADC	11.65	2.05–66.28	0.76			
Mean ADC	45.63	5.14–404.97	0.85			
	Reader 1			Reader 2		
Signal heterogeneity on T1-weighted imaging	1.62	0.49–5.40	0.56	2.11	0.64–6.95	0.59
Signal heterogeneity on T2-weighted imaging	NA	NA	NA	NA	NA	0.51
Shape	6.80	1.44–32.20	0.65	3.33	0.92–12.06	0.62
Margin			0.81			0.79
Partly well-defined	NA	NA		14.58	2.28–93.16	
Ill-defined	NA	NA		NA	NA	
Split fat sign	22.50	3.97–127.40	0.75	19.20	4.40–83.73	0.81
Fascicular sign	4.58	1.30–16.18	0.68	12.86	3.17–52.09	0.78
Target sign	9.13	1.09–76.86	0.66	8.24	1.64–41.47	0.71
Perilesional edema	NA	NA	0.78	NA	NA	0.78
Eccentric to the nerve	0.20	0.05–0.81	0.68	0.79	0.21–2.99	0.52
Enhancement	1.41	0.41–4.76	0.54	NA	NA	0.62
Hemorrhage	2.35	0.60–9.26	0.58	1.21	0.31–4.78	0.52
Cystic change	1.28	0.39–4.20	0.53	1.21	0.31–4.78	0.52
Bone destruction			0.57			0.62
Remodeling	1.36	0.22–8.52		0.73	0.07–7.22	
Destruction	2.73	0.48–15.58		11.64	1.17–115.59	

ADC, apparent diffusion coefficient; *NA*, not applicable

In our results, both the minimum and mean ADC values were significantly lower in MPNSTs than in BPNSTs, with the AUC of the ROC curve of the mean ADC value being slightly higher than that of the minimum ADC value (mean ADC value, 0.846; minimum ADC value, 0.759). The threshold values for the minimum and mean ADC values were 0.89×10^{-3} mm^2/s and 1.15×10^{-3} mm^2/s, respectively. Furthermore, the mean ADC value was identified as an associated factor in the bootstrapping model. This seems to be in contrast to previously reported results, which showed the minimum ADC value to be a better predictor of the risk of MPNSTs than the average ADC value [10]. We speculate that this difference may be caused by different methods for drawing the ROIs. While Demehri et al selected the largest circle or ellipse ROI enclosed entirely within the tumor [10], we selected ROIs according to the most restricted area within the tumors on visual assessment, because we determined that the areas showing low ADC values are more likely to contain malignant cells [14]. We also used in-house software to measure the ADC values, to avoid technical errors, and to facilitate

the inclusion of images from different institutions, which may also have resulted in differences.

A large tumor size is a feature of malignant soft tissue tumors, including MPNSTs [5, 7, 10]. Demehri et al [10] reported that the average tumor diameter of MPNSTs was significantly larger than that of BPNSTs, but that the maximum diameter of MPNSTs was not. They suggested that the reason for this is that BPNSTs may have a longer maximum diameter along the nerve of origin, but that the average diameter incorporating the lengths in the other two planes is smaller than the maximum diameter alone. Our study demonstrated that tumor diameters of MPNSTs and BPNSTs were significantly different in all directions, and that the frequency at bootstrap sampling was relatively higher than those of the other variables; however, the average diameter and the maximum diameters on all three planes were not found to be independent imaging findings.

Our results support the fact that DWI could complement the weakness of conventional MRI for differentiating benign and malignant PNSTs, when both PNSTs show similar

**Table 5** The selection proportions among 1000 bootstrap samples

Variable	Inclusion percentage (%)	
	R1	R2
Size		
Craniocaudal	28.7	18.6
Anteroposterior	5.3	7.3
Transverse	6.3	11.3
Average	19.4	23.1
Minimum ADC	17.7	8.9
Mean ADC	59.4	42.6
Signal heterogeneity on T1-weighted imaging	2.1	2.1
Signal heterogeneity on T2-weighted imaging	NA	NA
Shape	0.7	1.1
Margin	NA	NA
Split fat sign	40.1	66.1
Fascicular sign	4.3	25.9
Target sign	4.4	3.1
Perilesional edema	NA	NA
Eccentric to the nerve	21.8	3.0
Hemorrhage	1.8	0.1
Cystic change	4.6	0.3
Bone destruction	NA	NA

ADC, apparent diffusion coefficient; *NA*, not applicable

morphologic MRI features. DWI can provide the functional information about water diffusivity at the cellular level, resultantly aiding in differentiation of tumor cellularity. Diffusion tensor imaging, which is a subtype of DWI, can measure the direction of water diffusion in addition to the degree of diffusion. This technique with fiber tractography could allow direct delineation of fascicular course and integrity of the nerves, even in cases of PNSTs, which could be helpful in surgical planning for tumor resection [14].

This study has several limitations. First, it is of a retrospective nonrandomized design with a relatively small number of patients. Nevertheless, this study included a larger number of patients than previous similar studies. The MRI examinations were performed using different MR scanners at two different institutions, which could have affected the absolute ADC values. In previous studies, difference in magnetic field strength or MRI construction was reported to affect DWI and ADC values [22–24]. Second, there was a relatively high rate (32.7%, 18/55) of MPNSTs, which was much higher than the incidence in the general population. This is probably because we included cases that were pathologically confirmed at the tertiary institutions, which might have limited the generalizability. Third, our identified ADC cut-off values were not tested in a separate cohort to verify that they were optimal, nor was the predictive value of the combined MRI features tested on an independent data set. Further prospective multicenter

Fig. 3 A 41-year-old male with peripheral nerve sheath tumor in the left thigh. **a** Sagittal T1-weighted imaging shows the soft tissue mass with an oval shape and well-defined margin. The split fat sign (arrows) is evident. **b** Axial fat-suppressed T2-weighted imaging shows heterogeneous signal intensity without a target or fascicular sign. There is no edema around the tumor. **c** CEFST1WI shows inhomogeneous enhancement. **d** The ADC map has a mean ADC value of 1.353×10^{-3} mm²/s. The white drawing indicates the ROI for the ADC measurements. This case was read as indeterminate PNST, and the possibility of malignancy could not be ruled out. This tumor was surgically removed and pathologically confirmed as schwannoma
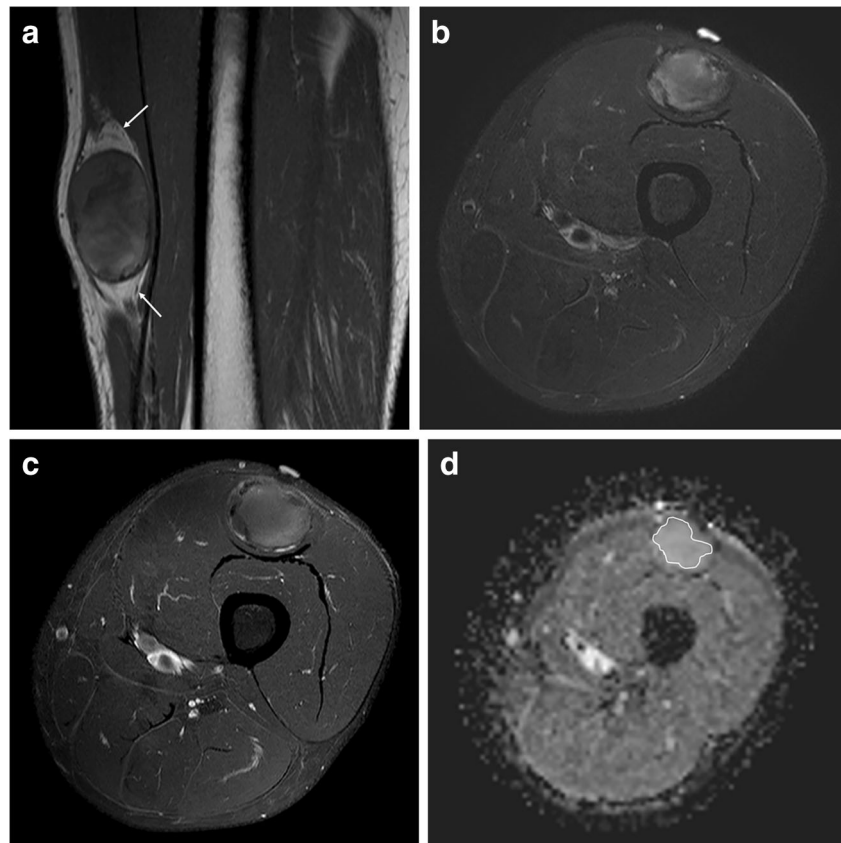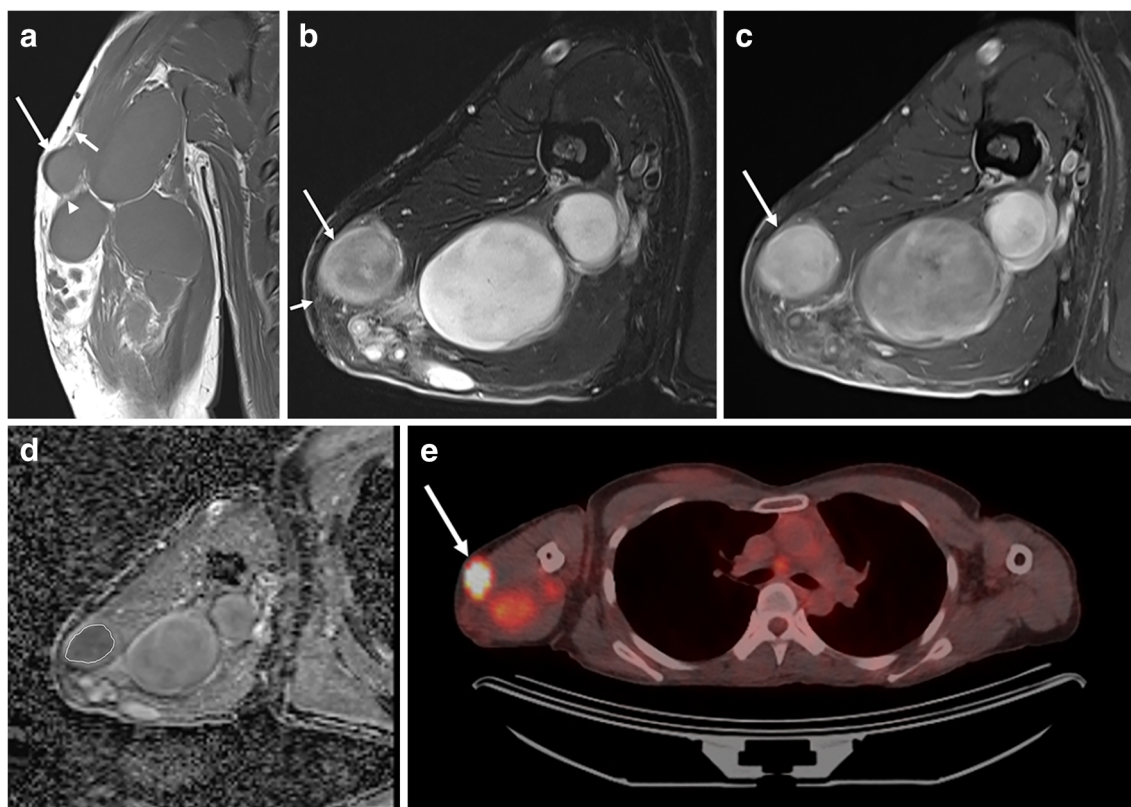
Fig. 4 A 31-year-old female with neurofibromatosis type 1. **a** Coronal T1-weighted imaging shows a number of peripheral nerve sheath tumors in the right upper arm. The soft tissue mass located in the most lateral aspect of the upper arm (long arrow) shows no definite fat split sign distal to the tumor (arrow heads), but a slightly obliterated fat signal in the proximal area of the tumor (short arrow). **b** Axial fat-suppressed T2-weighted imaging reveals more than three tumors in the right upper arm. The tumor located in the lateral aspect (long arrow) has faintly increased peritumoral signal (short arrow) at the posterior aspect. **c** This mass (arrow) is homogenously enhanced on CEFST1WI. **d** On the ADC map, the ROI shows diffusion restriction with an ADC value of 1.093×10^{-3} mm^2/s. **e** The tumor (arrow) demonstrates high metabolic activity on PET/CT (maximum standard uptake value, 12.7). This tumor was surgically removed and pathologically confirmed as a malignant peripheral nerve sheath tumor

studies with larger numbers of patients are warranted to consolidate our findings.

We conclude that benign and malignant PNSTs showed different imaging features on conventional MRI and DWI. Among them, the absence of a split fat sign and the mean ADC value were found to be associated with the diagnosis of MPNSTs. The combination of these two findings could be useful for discriminating between benign and malignant PNSTs.

Compliance with ethical standards

Guarantor The scientific guarantor of this publication is Min Hee Lee.

Conflict of interest The authors of this manuscript declare no relationships with any companies, whose products or services may be related to the subject matter of the article.

Statistics and biometry One of the authors has significant statistical expertise.

Informed consent Written informed consent was waived by the Institutional Review Board.

Ethical approval Institutional Review Board approval was obtained.

Methodology
• retrospective
• diagnostic or prognostic study
• multicenter study

References

1. Murphey MD, Smith WS, Smith SE, Kransdorf MJ, Temple HT (1999) From the archives of the AFIP. Imaging of musculoskeletal neurogenic tumors: radiologic-pathologic correlation. Radiographics 19:1253–1280
2. Kransdorf MJ (1995) Benign soft-tissue tumors in a large referral population: distribution of specific diagnoses by age, sex, and location. AJR Am J Roentgenol 164:395–402
3. Grobmyer SR, Reith JD, Shahlaee A, Bush CH, Hochwald SN (2008) Malignant peripheral nerve sheath tumor: molecular pathogenesis and current management considerations. J Surg Oncol 97:340–349

4. Wu JS, Hochman MG (2009) Soft-tissue tumors and tumorlike lesions: a systematic imaging approach. Radiology 253:297–316

5. Wasa J, Nishida Y, Tsukushi S et al (2010) MRI features in the differentiation of malignant peripheral nerve sheath tumors and neurofibromas. AJR Am J Roentgenol 194:1568–1574

6. Bhargava R, Parham DM, Lasater OE, Chari RS, Chen G, Fletcher BD (1997) MR imaging differentiation of benign and malignant peripheral nerve sheath tumors: use of the target sign. Pediatr Radiol 27:124–129

7. Li CS, Huang GS, Wu HD et al (2008) Differentiation of soft tissue benign and malignant peripheral nerve sheath tumors with magnetic resonance imaging. Clin Imaging 32:121–127

8. Ogose A, Hotta T, Morita T et al (1999) Tumors of peripheral nerves: correlation of symptoms, clinical signs, imaging features, and histologic diagnosis. Skeletal Radiol 28:183–188

9. Levine E, Huntrakoon M, Wetzel LH (1987) Malignant nerve-sheath neoplasms in neurofibromatosis: distinction from benign tumors by using imaging techniques. AJR Am J Roentgenol 149:1059–1064

10. Demehri S, Belzberg A, Blakeley J, Fayad LM (2014) Conventional and functional MR imaging of peripheral nerve sheath tumors: initial experience. AJNR Am J Neuroradiol 35:1615–1620

11. Priola AM, Priola SM, Parlatano D et al (2017) Apparent diffusion coefficient measurements in diffusion-weighted magnetic resonance imaging of the anterior mediastinum: inter-observer reproducibility of five different methods of region-of-interest positioning. Eur Radiol 27:1386–1394

12. Sung J, Kim JY (2017) Fatty rind of intramuscular soft-tissue tumors of the extremity: is it different from the split fat sign? Skeletal Radiol 46:665–673

13. Matsumine A, Kusuzaki K, Nakamura T et al (2009) Differentiation between neurofibromas and malignant peripheral nerve sheath tumors in neurofibromatosis 1 evaluated by MRI. J Cancer Res Clin Oncol 135:891–900

14. Mazal AT, Ashikyan O, Cheng J, Le LQ, Chhabra A (2019) Diffusion-weighted imaging and diffusion tensor imaging as adjuncts to conventional MRI for the diagnosis and management of peripheral nerve sheath tumors: current perspectives and future directions. Eur Radiol 29:4123–4132

15. Iwi G, Millard RK, Palmer AM, Preece AW, Saunders M (1999) Bootstrap resampling: a powerful method of assessing confidence intervals for doses from experimental data. Phys Med Biol 44:N55–N62

16. Kakkar C, Shetty CM, Koteshwara P, Bajpai S (2015) Telltale signs of peripheral neurogenic tumors on magnetic resonance imaging. Indian J Radiol Imaging 25:453–458

17. Chee DW, Peh WC, Shek TW (2011) Pictorial essay: imaging of peripheral nerve sheath tumours. Can Assoc Radiol J 62:176–182

18. Zhao F, Ahlawat S, Farahani SJ et al (2014) Can MR imaging be used to predict tumor grade in soft-tissue sarcoma? Radiology 272:192–201

19. Crombe A, Marcellin PJ, Buy X et al (2019) Soft-tissue sarcomas: assessment of MRI features correlating with histologic grade and patient outcome. Radiology 291:710–721

20. Fernebro J, Wiklund M, Jonsson K et al (2006) Focus on the tumour periphery in MRI evaluation of soft tissue sarcoma: infiltrative growth signifies poor prognosis. Sarcoma 2006:1–5

21. Banks KP (2005) The target sign: extremity. Radiology 234:899–900

22. Lavdas I, Miquel ME, McRobbie DW, Aboagye EO (2014) Comparison between diffusion-weighted MRI (DW-MRI) at 1.5 and 3 Tesla: a phantom study. J Magn Reson Imaging 40:682–690

23. Saremi F, Jalili M, Sefidbakht S et al (2011) Diffusion-weighted imaging of the abdomen at 3 T: image quality comparison with 1.5-T magnet using 3 different imaging sequences. J Comput Assist Tomogr 35:317–325

24. Rosenkrantz AB, Oei M, Babb JS, Niver BE, Taouli B (2011) Diffusion-weighted imaging of the abdomen at 3.0 Tesla: image quality and apparent diffusion coefficient reproducibility compared with 1.5 Tesla. J Magn Reson Imaging 33:128–135